CFD Model of an AUV inspired by the Cownose Ray

Giovanni Bianchi[1*], Simone Cinquemani[1], Paolo Schito[1], Francesco Braghin[1]
[1]Politecnico di Milano, Dipartimento di Meccanica, Via La Masa 1, 20156, Milano
ITALY

*giovanni.bianchi@polimi.it

ABSTRACT

The mechanics of fish swimming are of great interest because of their agility during maneuvers and their movements characterized by high energy efficiency. A better understanding of fish propulsion can lead to the design of novel and more performing autonomous underwater vehicles, which could find applications for seabed exploration, environmental monitoring, or surveillance purposes. This research aims at developing a model of the swimming dynamics of rays and mantas, focusing on the energy efficiency of their propulsion, and it is the starting point for bioinspired AUVs design. A CFD model of the swimming motion of a cownose ray has been implemented in OpenFOAM, simulating the acceleration of the fish from still to the steady-state velocity using an overset mesh. A custom code has been implemented for this analysis, which allows the 1-DOF dynamics of forward swimming to be solved with the fluid velocity and pressure. In contrast, the mesh motion due to the fin deformation is imposed. Several simulations have been carried out varying wavelength and frequency of the fin movement, and the effect of different kinematic parameters on swimming performances and wake structure has been studied. This research highlighted the presence of a Reverse Karman Street in the wake and of a leading-edge vortex for fin movements with great wavelength. Moreover, the energy efficiency of a self-propelled body has been calculated in a novel way, and in the case of cownose ray swimming, it resulted in being very high.

1 INTRODUCTION

Swimming was the first mode of movement on the planet. Aquatic species have evolved through natural selection for millions of years, implying that their propulsion techniques have reached a high efficiency [1]. This explains why researchers and engineers are interested in taking inspiration from such systems to propel autonomous underwater vehicles (AUVs) that might be used for marine life observation, search and rescue missions, or environmental monitoring of aquatic environments. Understanding the principles behind thrust production and why fish movements ensure exceptional agility and low power consumption is critical for developing this technology.

Batoid fishes, which include manta rays and stingrays, swim by moving their huge pectoral fins; this provides them with a significant advantage in terms of maneuverability and stealth; also, the endurance of batoid swimming indicates that their swimming motion is featured by high energy efficiency [2]. These properties are particularly appealing to AUVs, often built to maneuver quickly in tight locations and stay submerged for extended periods. This research aims to study the swimming dynamics of batoid fishes as a starting point for designing bioinspired AUVs. Since batoid fishes propel themselves with pectoral fins, their movement is classified as median paired fin [3]. Fin movement is essentially the development of a chordwise wave that travels in the opposite direction of fish motion. As a result of momentum conservation, this wave pushes the surrounding fluid backward, giving the fish a forward thrust.

Because of the complexity of the flow, a numerical approach is the most suitable to investigate the forces acting on the fins and the wake structure, to relate them to the kinematic parameters of fin deformation. Previous numerical studies about batoid fish swimming include the research of Fish [4], who investigated the efficiency of steady-state swimming of myliobatoid fishes with an immersed boundary element method; the

research of Liu [5], who analyzed the wake structure of a biomimetic ray robot swimming at a constant speed, the work of Zhan [6] regarding the gliding of a manta ray, and the numerical analysis of Sharp [7], who investigated the forces acting on a fin performing an undulatory motion using Multiparticle Collision Dynamics. The fluid dynamics of a deformable fin have been studied by Liu [8] and by Wei [9], who performed a dynamic analysis of the motion of a *Raja Eglanteria* coupling the CFD with a dynamic solver. Bottom carried out numerical simulations of swimming in stingrays analyzing vortices in the wake [10]. Similarly, Thekkethil studied the hydrodynamics of batoid fishes, highlighting that the cownose ray has one of the highest thrust coefficients among batoid fishes [11]. Huang performed a hydrodynamic simulation coupled with a 6DOF dynamics solver of a bioinspired robot with fins and propellers, studying the robot's stability during forward swimming and maneuvers [12].

The work presented in this article improves the results of the previous research analyzing the forward swimming of an AUV inspired by the cownose ray that accelerates from rest to the steady-state velocity. The deformation of the fin is imposed, whereas the forward swimming motion is calculated coupled with the pressure and velocity fields of the fluid. The wake structure and the swimming performances, in terms of thrust, efficiency, and steady-state velocity, are then related to the frequency and wavelength of fin movement. This analysis aims to explain the complex phenomena that allow the cownose ray to swim efficiently. For this purpose, a novel way to calculate efficiency has been proposed.

The article is organized as follows: Section 2 provides a description of cownose ray geometry and fin kinematics; Section 3 outlines the CFD model used for these dynamic analyses; in Section 4, the wake structure is analyzed; in Section 5, a definition of the efficiency for a swimming fish is proposed; in Section 6, the swimming performances with different kinematic parameters are compared; finally, Section 7 is dedicated to the conclusions.

2 FIN GEOMETRY AND KINEMATICS

The cownose rays adopt a median paired fin (MPF) locomotion, propelling by moving their large triangular pectoral fins [13]. The fin movement can be described as a traveling wave, and the cownose ray swimming is categorized as oscillatory since the number of waves along the fish's body is less than 0.5. Oscillatory locomotion is advantageous in cruising at high speed, whereas undulator fishes have better turning abilities, favored in maneuvering in narrow environments near the seabed or the coral reef. The cownose ray is featured by an average wave number of 0.4; thus, its swimming strategy is near the limit between oscillatory and undulatory swimming, so it is characterized by a good compromise between cruising speed and turning radius. This makes these fishes interesting for AUV design and development.

The size and the shape of the designed AUV are the same as those of a real cownose ray, as shown in Figure 1 [14] [15]. The cross-section of the fin is approximated as a series of symmetric airfoils tapering toward the fin tip: at the body center, the cross-section is approximated with a NACA 0020, at the midspan with a NACA 0015, and close to the fin tip with a NACA 0012 [16].

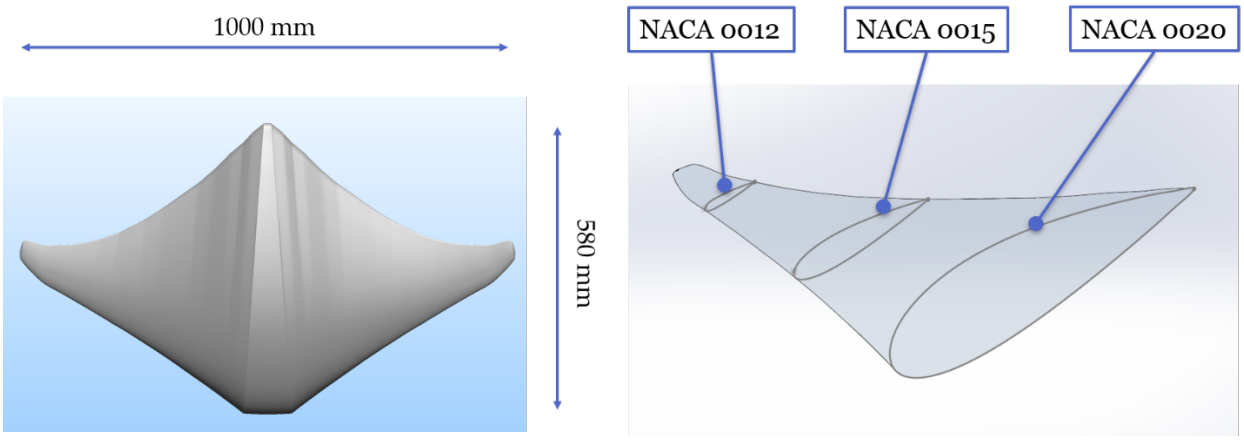

Figure 1: Shape and dimensions of cownose ray fins.

The kinematics of batoid fishes' swimming has been analyzed by Russo [17], who implemented a biomechanical kinematic model of the fin deformation. The cartilaginous structure of the fin is composed of radial segments connected with rotational joints. Considering θ the angle formed by each segment of the fin with the horizontal, it is possible to determine it as follows:

$$\theta(s,t) = \theta_{max}\, sin(\phi x + \psi s - \omega t) \tag{1}$$

where θ_{max} is the angle at the fin tip, s is the curvilinear abscissa the position of the cartilage segment from the fin root, x is the position from the leading edge, as shown in **Figure 2**, ϕ is the chordwise wave number divided by the body length of the fish, ψ is the spanwise wavenumber divided by the span length of the fin, x is the frequency of fin movement [17]. The wavenumbers ϕ and ψ are defined as follows:

$$\phi = \frac{2\pi}{\lambda_x} \qquad \psi = \frac{2\pi}{\lambda_s} \tag{2}$$

where λ_x is the wavelength of the wave traveling in a longitudinal direction, whereas $\lambda_s$is the wavelength of the wave propagating spanwise from the fin root to the fin tip [17]. Since the fin is composed of hundreds of segments and joints [17], it is reasonable to consider the fin deformation as continuous.

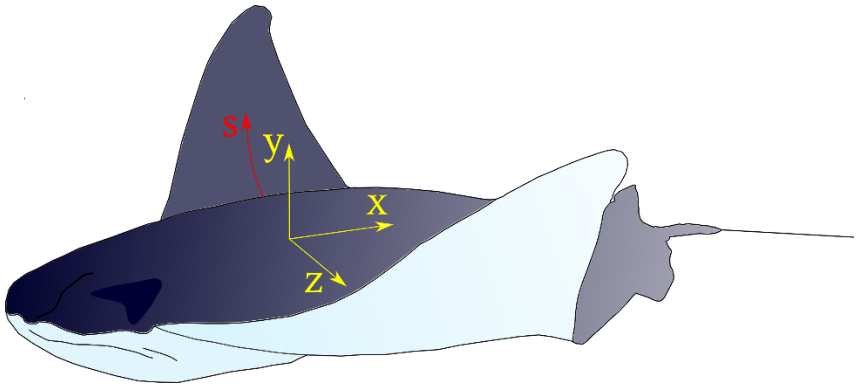

Figure 2: Representation of the coordinates x and s, used in Eq. (1), on the fin

The tip deflection lag, determined by the spanwise traveling wave, is due to the flexibility of the fin itself and gives a less important contribution to thrust than the chordwise wave ***[18]*** ; therefore, ***ψ*** can be neglected

in this analysis. It has been hypothesized that the tip lag effects reduce losses due to the tip vortices ***[4]***; however, it will be studied in future research.

Lying on this assumption $\theta(s,t)$ becomes:

$$\theta(s,t) = \theta_{max}\, sin(\phi x - \omega t) \tag{3}$$

and the y and z coordinates of each point of the fin are computed as:

$$\begin{cases} y(s,t) = \int_0^s \sin\theta(\sigma,t)\, d\sigma = \dfrac{1-\cos[\theta_{max} s\ \sin(\phi x - \omega t)]}{\theta_{max}\ \sin(\phi x - \omega t)} \\ z(s,t) = \int_0^s \cos\theta(s,t)\, d\sigma = \dfrac{\sin[\theta_{max} s\ \sin(\phi x - \omega t)]}{\theta_{max}\ \sin(\phi x - \omega t)} \end{cases} \tag{4}$$

Equation 4 represents a wave traveling backward, pushing water in the opposite direction to forward motion. Therefore, the fish is subject to a forward thrust because of momentum conservation. The magnitude of this thrust depends on the speed at which the fluid is accelerated backward by the wave. A necessary condition for generating a propulsive force is chordwise to travel at a higher speed than the swimming velocity of the fish.

3 CFD MODEL DESCRIPTION

The CFD model of cownose ray swimming has been implemented using the open-source software OpenFOAM, and the simulation is performed using an overset mesh. Thus, two mesh grids are merged: the first includes the whole domain and remains still, whereas the second consists of a portion of fluid around the fish and moves with it. These two meshes are superimposed in the same space, and the software can interpolate between the overlapping elements and find a unique solution [19]. The movement of the overset mesh surrounding the fish is the superimposition of two motions: forward swimming and fin deformation. As far as the fin deformation is concerned, every point of the overset mesh is moved according to Equation 4, so the mesh deformation corresponds to the fin movement depending on fin kinematics which is known in advance and imposed. The mesh deformation caused by the fin motion is imposed on all points belonging to the overset mesh by including Equation 4 into the motion; the fish and its surrounding mesh are treated as a rigid body for forward swimming. The dynamics along the longitudinal axis of the fish are solved with a Newmark solver featured by $\beta = 0.25; \gamma = 0.5$. The only degree of freedom left to the fish is the forward displacement since all the other DOFs are constrained. Hence, every time-step, the fins are moved, deforming the internal mesh, the solver calculates the forces acting on the fins, and the forward displacement of the fish is calculated.

The solved equations are unsteady Reynolds-averaged Navier–Stokes (URANS), and the solver used in OpenFOAM is overPimpleDyMFoam, able to solve unsteady, incompressible, turbulent flows with an overset mesh. The domain is shown in **Figure *3***, where the fixed mesh is colored blue, and the moving mesh is red. The background domain is composed of 300,000 (200x30x50) hexahedral cells, with a gradual refinement toward the area occupied by the overset mesh. Its dimensions are 5mx3mx2m, as shown in **Figure *4***(a). The moving mesh is obtained using snappyHexMesh on a 0.6mx0.2mx1.1m block, with three levels of refinement on the surface of the fish, resulting in a mesh of 1,462,199 cells, as shown in **Figure *4***(b). The adopted interpolation scheme is cellVolumeWeight, and the cells at the boundary of the overset mesh have similar dimensions to cells of the background mesh to reduce interpolation errors.

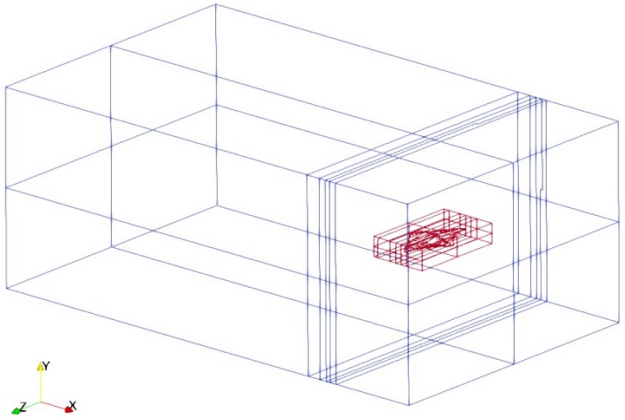

Figure 3: Domain of the CFD simulation

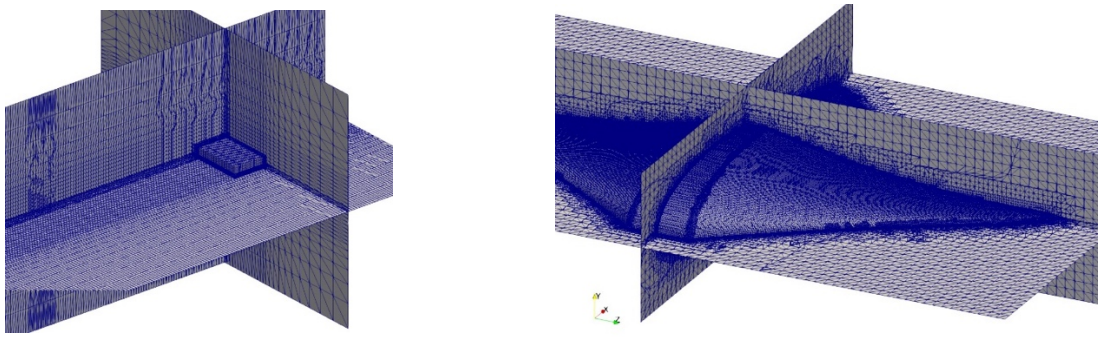

(a) Background mesh **(b) Overset mesh**

Figure 4: Mesh used in the CFD simulation

The mesh size sensitivity analysis results are shown in **Figure 5**(a), where the velocities obtained with different mesh grids are presented. It is possible to appreciate that the results are independent of mesh size since the average error between the normal and the most refined mesh is 1.25%.

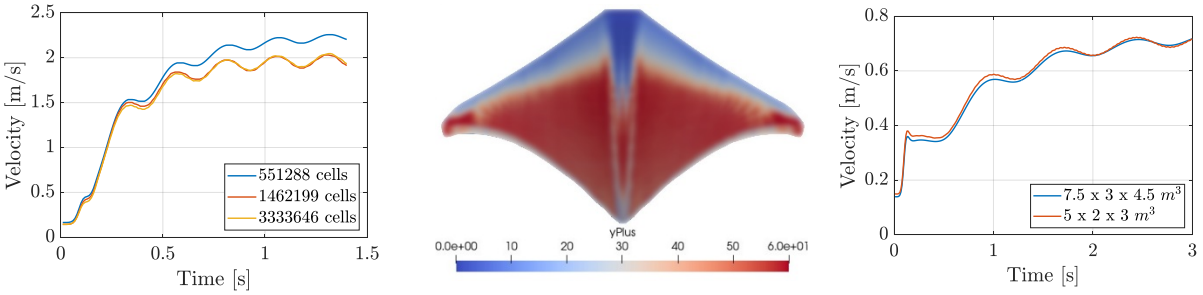

(a) - velocity obtained with cells of different sizes **(b) – y+ on the surface of the fish,** **(c) - velocity obtained with domains of different sizes**

Figure 5: Mesh grid sensitivity analysis

In **Figure 5**(b), the surface of the fish is colored with y^+ for the adopted mesh: the values are smaller than 300, and standard wall functions are used with a $k-\omega\ SST$ turbulence model. An analogous analysis has

been carried out to evaluate the independence of the results from the domain size. The results are plotted in **Figure 5**(c), where it is possible to note that by enlarging the domains, the velocity difference is negligible. For this analysis, the dimensions of the overset domain have been changed proportionally to the background domain.
At the beginning of the simulation, the fins are in their undeformed configuration, and the pressure and the velocity of the fluid are zero all over the domain. Zero-gradient velocity boundary conditions are applied to the sides of the domain, and a moving wall velocity condition is applied on the surface of the cownose ray. Pressure is set to a fixed value of zero on one extremity of the domain, and a zero-gradient condition is applied to all the other boundaries.
The Reynolds number characterizing the flow is necessary information prior to the simulation since it is needed to set the values of the turbulence closure parameters. However, the swimming velocity of the fish is still unknown; therefore, it is possible to estimate the Reynolds number from the Swimming number, as reported in Equation 5 [20].

$$Re \approx Sw = \frac{\omega A L}{\nu} \tag{5}$$

where ω is the fin flapping frequency, A is the amplitude of the fin tip displacement, L is the average chord length of the fin, and ν is the kinematic viscosity of water. The Reynolds number characterizing cownose ray swimming is $\sim 10^5$ for all possible kinematic parameters of fin motion.
The simulations have been run on a desktop workstation with an Intel® Xeon® Silver 4214 CPU @2.20 GHz and parallelizing the calculations on 24 logic processors. The duration of each simulation is different because the time to reach the steady-state velocity depends on the kinematic parameters of fin motion, and on average, each simulation takes about 430 hours. The time required by this kind of simulation is great because high complexity in the model is necessary, as it is impossible to obtain reliable results about the interaction of the fins with the fluid with lower fidelity methods. A 3D analysis is required for this kind of fish because the fin movement and the fin shape are variable along the lateral dimension. Thus, a spanwise flow on the fin is generated, which is responsible for generating vortices near the fin tip. The analysis of vortices around the fins and in the wake is fundamental to understanding the propulsion mechanism of fish swimming. The importance of vortices explains why the numerical analysis should also account for unsteadiness in the flow, which is an intrinsic property of the hydrodynamics of fish swimming, which relies on the periodic motion of the fins. Therefore, even during steady-state swimming, the velocity of the fish is not constant, but it oscillates around an average value because of the periodicity of thrust generation. This makes it impossible to study the fish still and immersed in a constant velocity flow because there would not be the equilibrium of forces. Therefore, an overset mesh is necessary to consider a relative motion with a variable velocity between the fish and the water.

This CFD model thus can solve the dynamics of a deformable body immersed in a fluid, as long as the deformation of the body is known in advance. This is the case of fish swimming, as the deformation of the fins is a prescribed movement, actuated by a considerable number of muscles and joints characterizing the structure of the fins. Hence, this model can be applied to any other fish or a bioinspired autonomous vehicle, whose kinematics is predefined. A different but similar application of this model could be the study of bird and insect flying or any flying object with actuated deformable wings since the nature of the problem is analogous to fish swimming. This CFD model can also investigate the dynamics of systems of rigid bodies that have predefined motion laws.

4 STRUCTURE OF THE WAKE

The description of the thrust generation principle and the wake structure shows the simulation with $\omega = 4\pi$ rad/s, and $\lambda_x = 2.5$ body length (BL). Still, the qualitative description of the results can be extended to all

the other cases. Thrust generation is concentrated on the external parts of the fins, moving with higher amplitude, whereas the central part of the body generates most of the drag. The contribution to thrust generation over the surface of the fin is shown in **Figure 6**. A negative value means a contribution to thrust, and a positive value represents drag.

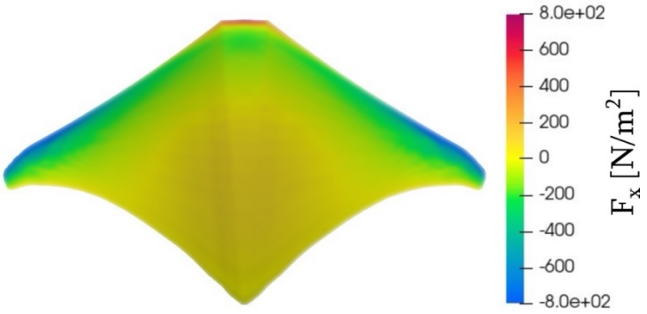

Figure 6: Force in the swimming direction on the bottom side during the upstroke

Figure 7 displays the pressure distribution during the upstroke and the downstroke in the plane at the midspan of the fin, shown in **Figure 7**(a). The fin movement generates a wide area of negative pressure in front of the fish, which is pushed forward by this pressure difference. The propulsive force is generated during both upstroke and downstroke with equal values since the fin profile and its motion are symmetric. Thus, during a flapping cycle, thrust generation is subject to a sinusoidal variation with a double frequency with respect to the flapping frequency. The generation of propulsive force is proportional to the fin velocity; thus, it is maximum in the midpoint of flapping, and it is minimum at the upper and lower limits of the stroke.

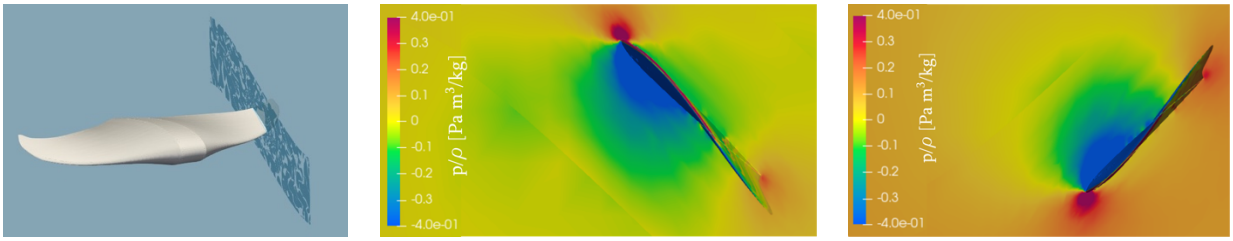

(a) – Midspan plane of the fin **(b) - Upstroke** **(c) - Downstroke**

Figure 7: Pressure distribution in a midspan plane of the fin

The thrust generated during four periods of fin flapping is shown in Figure 8(a). At the beginning of the simulation, when the fish is accelerating, there is a propulsive net force over one period, whereas, when it has reached the steady state, the average force over the period is null. As shown in Figure 8(b), the steady-state velocity is reached after a few cycles, and the velocity oscillations around the average do not exceed 5%. The cownose ray velocity is non-dimensionalized with respect to its dimensions, and it is presented in body length per second (BL/s), where the body length is 0.58 m, as shown in Figure 1.

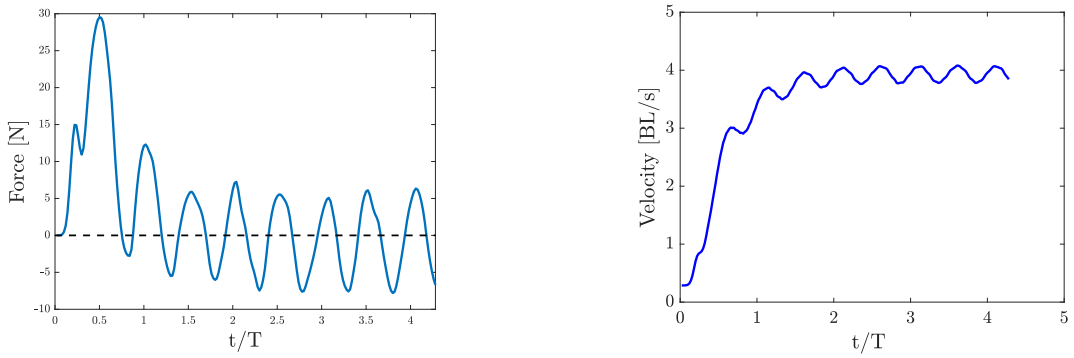

(a) Force in the swimming direction **(b) – Velocity of the fish**

Figure 8: Thrust and velocity during four periods

Studying of the vortices in the wake allows understanding of how the fluid is moved by the fin and the principles behind this locomotion strategy. The vortices in the wake, identified with the contour of the surface with $\lambda_2 = 0$, are displayed in **Figure 9**.

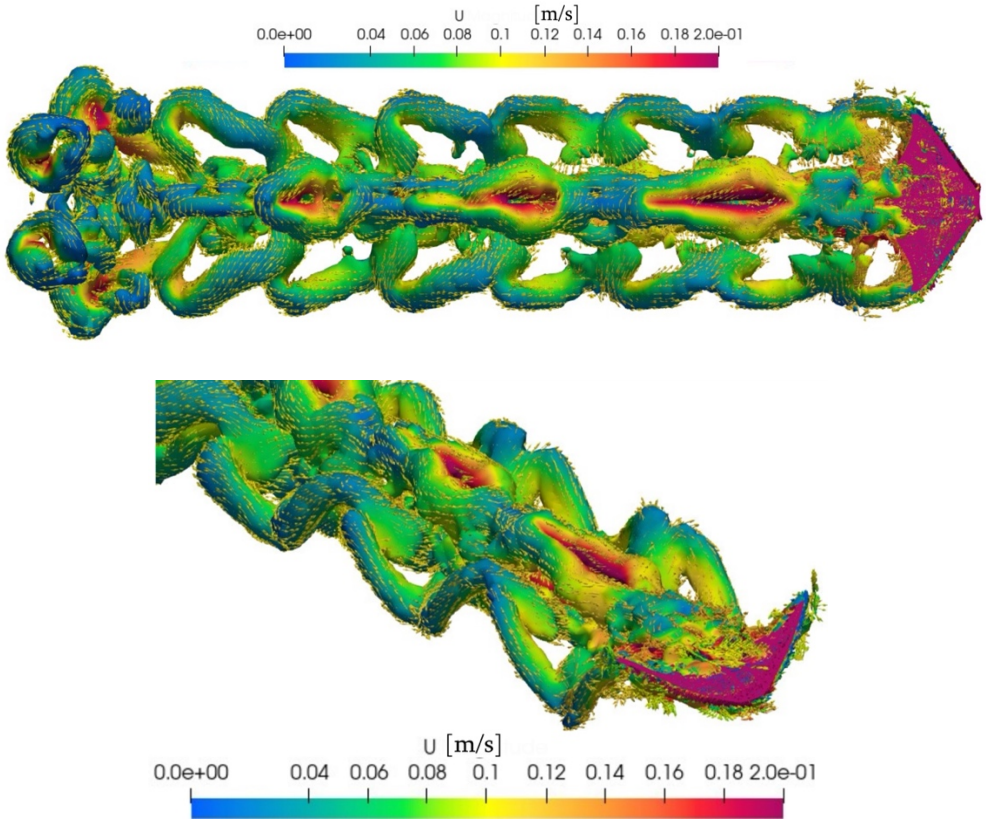

Figure 9: Vortices in the wake with vorticity vectors

These vortices can be divided into four main parts:

- fin tip vortices;
- fin midspan vortices;
- body center vortices;

- leading-edge vortices.

The fin tip and the body center vortices result from the spanwise flow. In contrast, the vortices formed behind the midspan of the fins are the result of the thrust-generating mechanism characteristic of this locomotion strategy. The obtained results are consistent with the results obtained experimentally by Clark [21] and by Dewey [22], who performed experiments on a batoid-inspired fin actuated in a traveling wave motion. They have highlighted that vortices in the wake have an alternate sign, and they are arranged similarly to a reverse Karman street, and they have put in evidence a vortex around the fin tip.

4.1 Reverse Karman Street

Vortices are shed in the wake at each half flapping period when the fin reaches the top or the bottom of its movement, and they rotate clockwise or counterclockwise depending on whether the fin has performed an upstroke or a downstroke [5]. Observing the wake structure in a plane perpendicular to the fin span shown in **Figure *10***, it can be noticed that vortices are arranged like in a reverse Karman Street, with counterclockwise vorticity on the top and clockwise vorticity at the bottom, as the fish swims leftward. This vortex arrangement creates a propulsive jet in the center of the wake, whereas a counterflow is present in the surrounding volume. When the fish swims at a constant speed, the jet stream and the counterflow are balanced, and the net streamwise momentum in the wake is null [23]. Each fin section is moving like heaving and pitching airfoil [24].

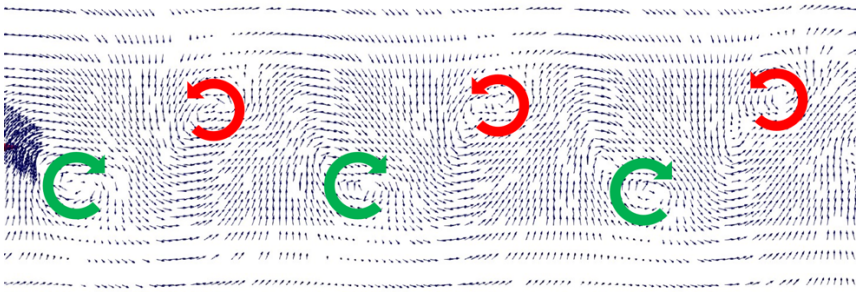

Figure 10: Reverse Karman Street in the wake

Although vortices cause dissipations, it is unavoidable that some vortices are generated when a body generates a force in a viscous fluid. The vortices of the reverse Karman Street are a direct consequence of this kind of motion, responsible for thrust production [24]. Therefore, although it is desirable to keep them as small as possible, they result from a thrust-producing movement of high energy efficiency. As shown in **Figure *11***, with the fish swimming from right to left, during acceleration, the wake presents a momentum surplus in the opposite direction to swimming. On the top, velocity vectors in the wake are shown; the water is pushed backward by fin motion and alternately upward and downward following the fin displacement. In the beginning, when the acceleration is more significant, the amplitude of velocity vectors is higher. At the bottom, the velocity component in the swimming direction is presented in a color scale. It is possible to note that a propulsive jet stream is present in the center, whereas on the top and at the bottom, in correspondence of vortices, some water moves in the opposite direction.

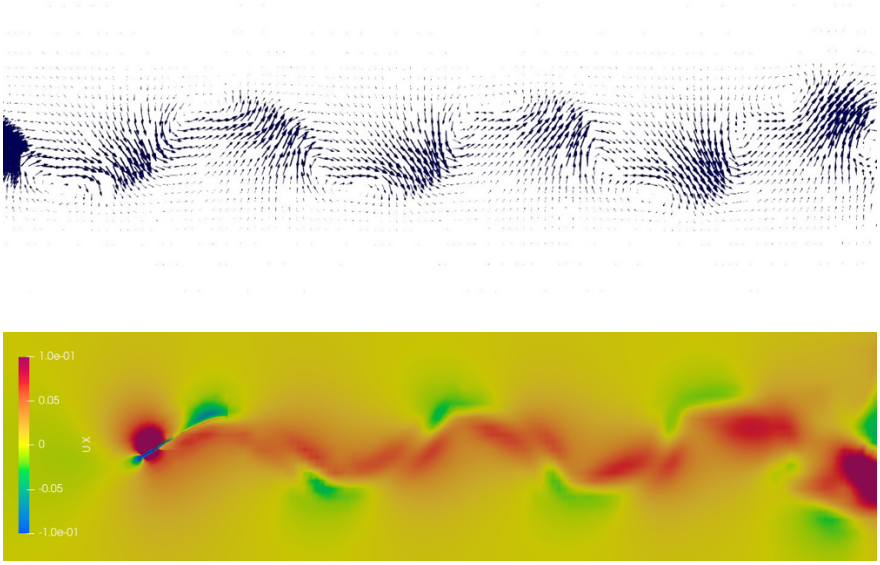

Figure 11: Velocity vectors and velocity component in the swimming direction in a fin midspan plane

4.2 Fin tip vortices

The fin tip vortices, shown in **Figure *12***, are formed by the pressure difference between the two sides of the fin. During the downstroke, the fin motion generates negative pressure on the upward-facing side; thus, the fluid on the downward-facing side tends to rotate around the fin tip and move to the other side, generating a vortex. The exact mechanism is repeated during downstroke with a vortex spinning in the opposite direction. The curvature of the fin reduces the strength of this vortex, making the fin tip act as a winglet and obstructing the passage of water from one side to the other.

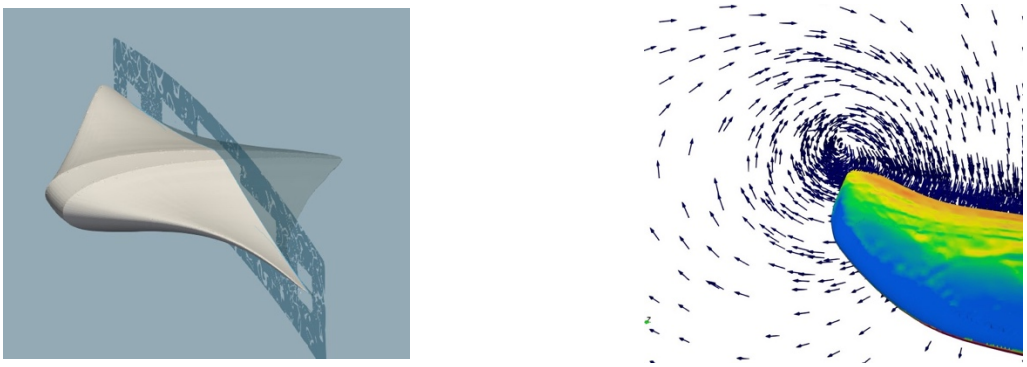

(a) – Plane behind the fin tip **(b) – Fin tip vortex**

Figure 12: Fin tip vortex during a downstroke

4.3 Body center vortices

The vortices forming near the body center are displayed in **Figure *13***. They arise because of the alternate inward and outward motion of the fin tips. These vortices rotate in opposite directions on the two sides of the fish, and they reverse their vorticity between upstroke and downstroke.

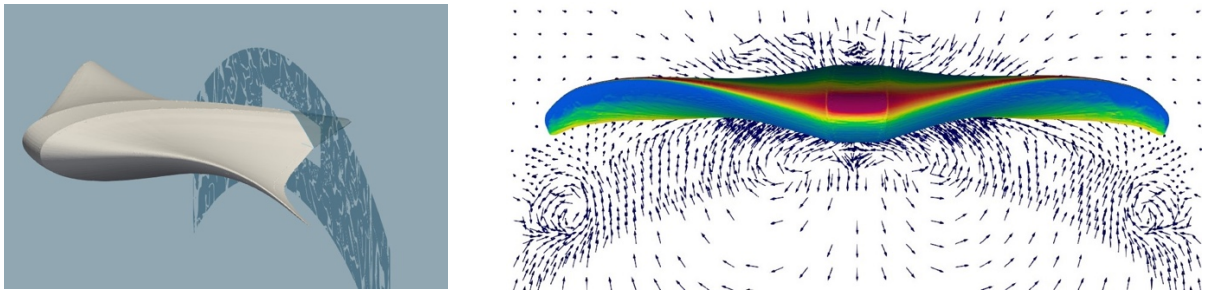

(a) – Plane near the tail (b) – Vortices near the center of the body

Figure 13: Body center vortices

4.4 Leading-edge vortices

A vortex on the leading-edge (LEV) of the fins is a characteristic of animals swimming with lift-based propulsion, like carangiform and thunniform fishes [10] [25]. The fin acts as a heaving and pitching airfoil with a high angle of attack, which generates a lift force in the front of the fin that pulls the fish forward. A stable leading-edge vortex is very common in nature since it enhances lift generation and is observed on flying insects' wings [10].

In this work, the swimming performances with different wavelengths are compared, and the influence of this parameter on the LEV is discussed. **Figure *14***(a) shows the streamlines of absolute velocity on the fin tip for a short wavelength during a downstroke. Only the fin tip vortex can be observed, and no vortices are present on the leading edge. Looking at **Figure *14***(b), where the relative velocity vectors are represented, the same observations can be made since the velocity vectors always remain parallel to the swimming direction. The relative velocity is calculated as the difference of the speed of the fluid and the forward swimming velocity of the fish; it is different from the relative velocity between each section of the fin and the fluid since the fin is also moving in a vertical direction.

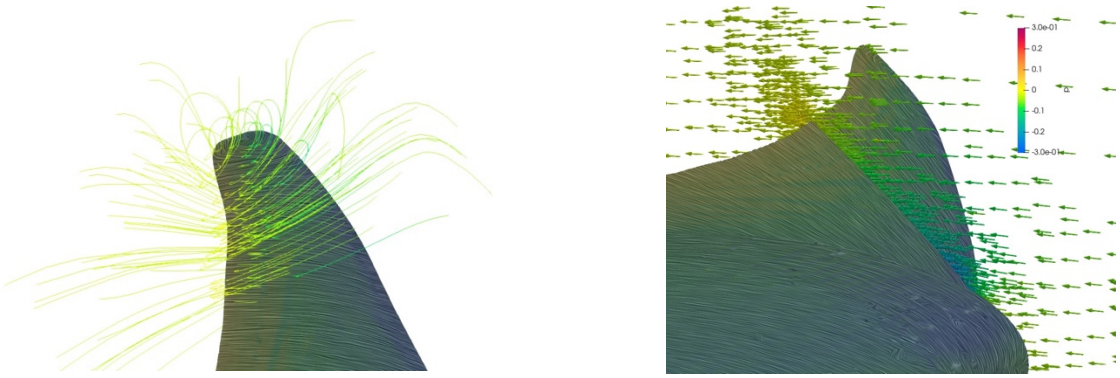

(a) – Streamlines near the fin tip (b) – Relative velocity vectors

Figure 14: Streamlines and relative velocity for $\lambda_x = 1.67\ BL$

On the other side, when the wavelength is larger, and the motion is oscillatory, a vortex near the leading edge forms. The streamlines of absolute velocity around the fin tip during a downstroke are shown in Fig. 16(a), highlighting the formation of a leading-edge vortex. The water near the leading edge flows from the top side to the bottom side, and it rotates, generating a vortex connected with the vortex around the fin tip. This vortex is responsible for developing a low-pressure area at its center, near the leading edge, which enhances thrust.

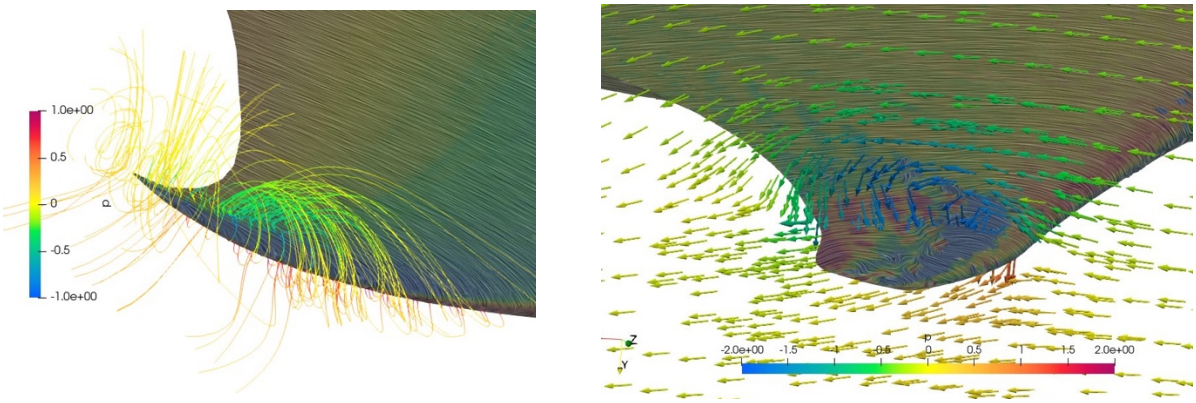

(a) – Streamlines near the fin tip **(b) – Relative velocity vectors**

Figure 15: Streamlines and relative velocity for $\lambda_x = 20\ BL$

The formation of an LEV for oscillatory fin motion of batoid fishes was also observed by Lu [26], who studied the movement of a manta ray, characterized by a longer wavelength than the cownose ray. They also have highlighted that the LEV strength increases with an increasing wavelength.

5 EFFICIENCY OF FIN PROPULSION

The conventional definition of propulsive efficiency is appropriate to systems where the propeller is separate from the main body; thus, it is straightforward to distinguish the thrust component from the drag. In contrast, in the case of a self-propelled body like a fish, fins' deformation is responsible for thrust and drag at the same time since the drag force is a function of the angle of attack of the fin, which is variable during fin movement. Hence, the traditional Froude efficiency of a swimming fish, shown in Equation 6, would be always zero because the net acting force in the swimming direction over a period is null [27], as thrust and drag at the steady state are equal and opposite. Since the swimming motion is unsteady, the efficiency can only be evaluated as the ratio between the average output and input power over a period.

$$\eta = \frac{\int_T F_x v_x \, dt}{\int_T P_{in} dt} \tag{6}$$

Therefore, a different definition of energy efficiency is required to assess the performance of a swimming fish. A parameter widely used in biology to measure the energy efficiency of other animals is the cost of transport, defined as the energy spent per unit distance traveled [28]. However, this coefficient is dimensional depending on the mass of the animal, so it is helpful to compare different gaits of the same fish. Still, it does not provide information about the absolute efficiency of the motion.

To quantify the propulsive efficiency of a fin, it is required to separate the contributions of thrust and drag. This work provides a novel definition of efficiency, suitable for self-propelled bodies like fishes. Since the data coming from the simulation allows distinguishing the contribution of pressure and viscous forces, it is possible to define efficiency properly. The input power P_{in} is the power spent by the fish to move its fins, and it is obtained as the scalar product between the forces acting on the fins and the relative velocity of the fins with respect to the fish body v_{rel}, i.e., the vertical and lateral components of velocity, as expressed in Equation 7. The forces acting on each fin element are the pressure force $p\boldsymbol{n}$, where $\boldsymbol{n}$ is the normal versor of the fin surface, and the viscous tangential stresses $\boldsymbol{\tau}$.

$$P_{in} = \int_A (p\boldsymbol{n} + \boldsymbol{\tau}) \cdot \boldsymbol{v_{rel}}\, dA \tag{7}$$

The useful output power P_{out} is the result of the pressure acting on the fins projected on the swimming direction. In contrast, the pressure acting on the rigid central body and the tangential stress acting on the whole surface contribute to the wasted power, as expressed in Equation 8.

$$P_{out} = \int_{A_{fins}} (pn_x)\, v_x\, dA \tag{8}$$

This definition of efficiency is indicative of how much power contributes to generating a propulsive force. The tangential forces acting on the surface result from dissipative viscous effects, and the pressure force acting on the central body is always resisting forward motion.

In **Figure *16***, the contribution of each of these forces during a few periods can be observed. When the fish has reached the steady-state velocity, the total force in the swimming direction (x) oscillates around a null mean value. It can be decomposed in a positive contribution given by the pressure force acting on the fins and a negative contribution constituted by the tangential forces and the pressure acting on the central body. When the fins reach the top or the bottom of their motion, they change direction, and, in this instant, their velocity is zero. Therefore, they do not generate any useful force on the surrounding fluid, and only drag is present.

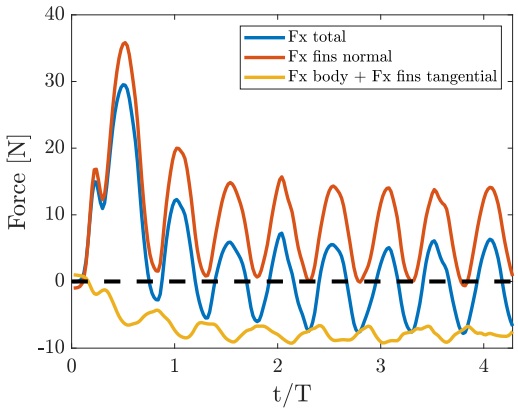

Figure 16: Forces acting on the fish along the swimming direction

6 INFLUENCE OF THE KINEMATIC PARAMETERS ON THE SWIMMING PERFORMANCE

Several dynamic analyses have been carried out, changing the frequency and the wavelength of fin motion to investigate the performances of these fishes and understanding the physical principle behind its efficiency. The amplitude of fin flapping is the same for all simulations.

6.1 Wavelength effect

The cownose ray is an oscillatory fish, and it moves its fins with a wave traveling at about 2.5 body lengths (BL) per second at about 1 Hz [29] [17]; however, it adjusts wavelength and frequency to tune maneuverability, power consumption, and acceleration according to its needs. In **Figure *17***(a), the velocity of the fish for

different wavelengths is presented. Increasing the wavelength, the steady-state velocity increases, then it reaches a maximum, and, with an extremely high wavelength, it decreases again. This occurs because a longer wavelength implies a higher wave propagation velocity; thus, water is pushed backward at a higher speed, providing more momentum to the fish. Nevertheless, a long wavelength implies that the fin is flat, pushing water more in a vertical direction than backward; therefore, it is more difficult to generate thrust. This result is consistent with the observation that batoid fishes with an oscillatory behavior, i.e., a longer wavelength, swim faster, and their motion is suitable to roam across the oceans, whereas fishes with an undulatory behavior, i.e., a shorter wavelength, are featured by small velocities and live in narrow environments [17]. When the wavelength is large enough, the effects of wavelength variations are minor because the number of waves on the fin, the reciprocal of the wavelength, is very similar. The efficiency of fish swimming is plotted in **Figure *17***(b) for different wavelengths λ. Swimming strategies involving a higher wavelength entail that the fin remains flatter, so the water is pushed more in a vertical direction. This is the reason why a shorter wavelength results in a more efficient swimming strategy. The efficiency is calculated averaging the power over a period, and it is meaningful only when the fish has reached the steady-state velocity.

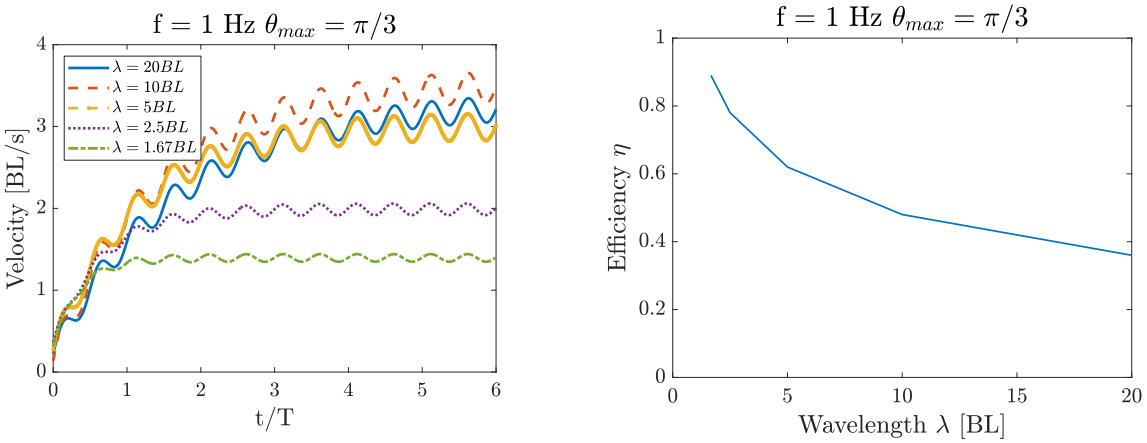

(a) - Velocity **(b) – Efficiency**

Figure 17: Velocity and energy efficiency of swimming at 1 Hz with different wavelengths

6.2 Frequency effect

In order to study the frequency effect on swimming performances, it has been chosen to perform simulations with different frequencies and with a wavelength of 2.5 BL/s. This number has been selected since it is a good trade-off between the velocity at the steady-state and the energy efficiency, as shown in the previous paragraph, and because it is close to the actual behavior of a cownose ray in nature [17] [29]. In **Figure *18***, the forward velocity of the fish swimming with different frequencies is presented, and it can be observed that the steady-state velocity is proportional to frequency, consistently with the results obtained by Huang [12]. This is a remarkable result because it means that the swimming of batoid fishes can be linearly scaled with frequency, and the efficiency is not affected by frequency variations, as shown in **Figure *18***.

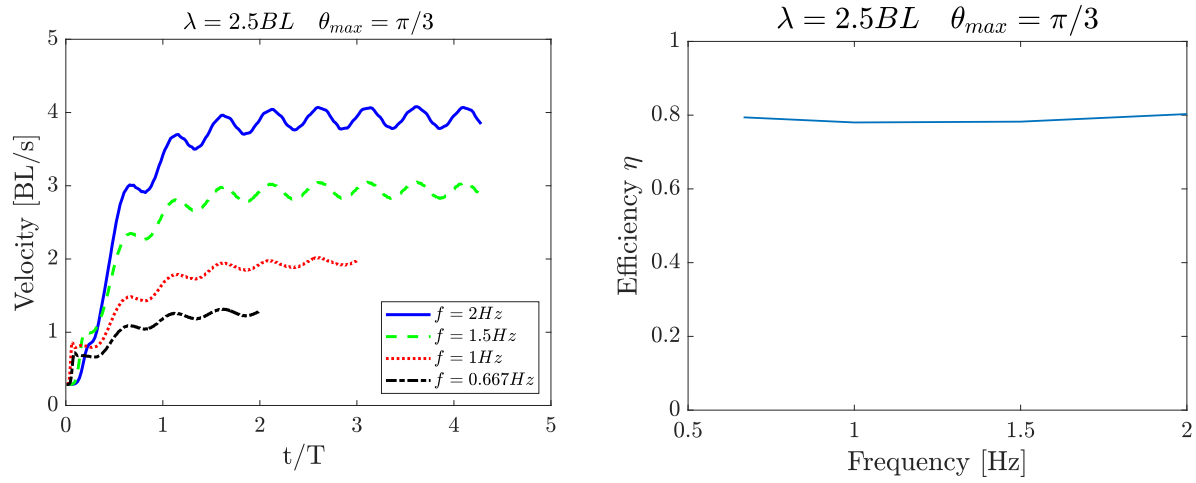

(a) - Velocity **(b) - Efficiency**

Figure 18: Velocity and energy efficiency of swimming with a wavelength of 2.5 BL with different frequencies

The effects of wavelength and frequency on swimming performances are summarized in **Figure *19***. The velocity increases linearly with frequency, and it has a maximum for a particular wavelength, and the efficiency only depends on wavelength. Therefore, in terms of energy consumption, the swimming of batoid fishes can reach high efficiencies, up to 89% for some swimming conditions, and to achieve an acceleration, it is more convenient to change the frequency instead of wavelength.

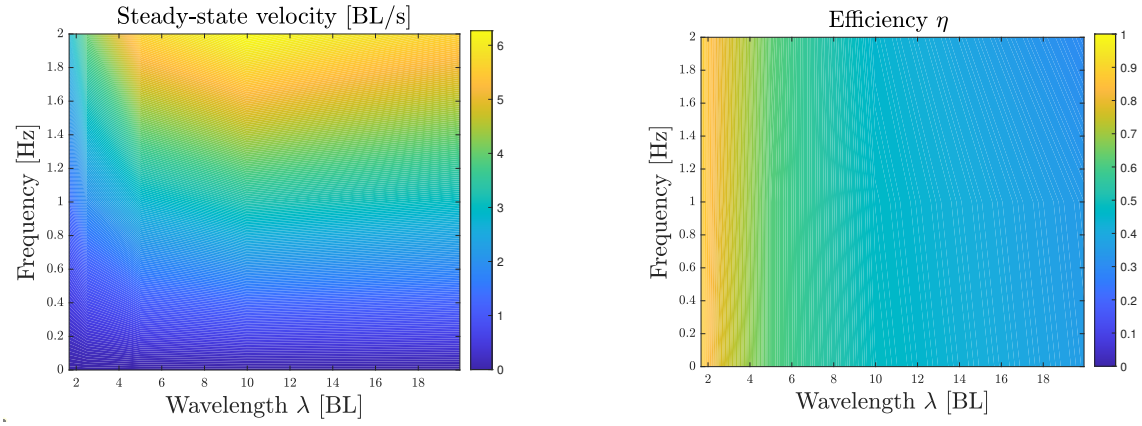

(a) – Steady-state velocity **(b) - Efficiency**

Figure 19: Steady-state velocity and efficiency for different wavelengths and frequencies

6.3 Angle of attack

Since the deformation of the fins of a cownose ray is featured by a small number of waves, about 0.4 [17], it is possible to consider every section of the fin as a heaving and pitching airfoil, and the angle of attack can be defined. The angle of attack α is the angle between the chord of the fin and the relative velocity of water with respect to the fin, as shown in Fig. 24(a), where ψ is the pitch angle of the fin section. The horizontal velocity of the fins v_x is the same for every section of the fin, whereas the vertical velocity v_y and the pitch angle ψ are different for every section of the fin since the fin tip motion has a larger amplitude than the fin root. Therefore, the angle of attack varies along the fin span. The angle of attack is the difference between the angle of the relative velocity and the pitch angle ψ.

$$\alpha = \psi - \tan^{-1}\frac{v_y}{v_x} \tag{9}$$

Neglecting the motion of the out-of-plane movement of fin section, which is smaller than the other two components, the relative velocity v_{rel} has two components: a horizontal component v_x equal to the forward velocity of the fish, and a vertical component v_y, which is $\dot{y}(s,t)$, the derivative of Equation 4. For a fin section, the velocity v_y is linearly dependent on frequency, and the forward velocity v_x is proportional frequency too. On the other side, a wavelength variation does not affect the velocity v_y, but it significantly changes the forward velocity v_x, as shown in **Figure *17***. Hence, the angle of the relative velocity does not depend on the frequency but only on the wavelength of fin motion. Furthermore, the pitch angle ψ too is independent of the frequency, and it is dependent only on wavelength. In particular, the larger is the wavelength, the flatter is the fin, and, as a consequence, the smaller is the pitch angle. Thus, the angle of attack of any section of the fin is a function of the wavelength of fin motion. In **Figure *20***, the variation of the angle of attack of a section near the fin tip over a period is presented.

A wavelength variation has two effects on the angle of attack: the first is due to the variation of ψ, the second is due to the different forward velocity. At the fin tip, the angle of attack is larger for longer wavelengths, meaning that when the fin is performing an upstroke, the angle of attack is negative, and it is positive during a downstroke.

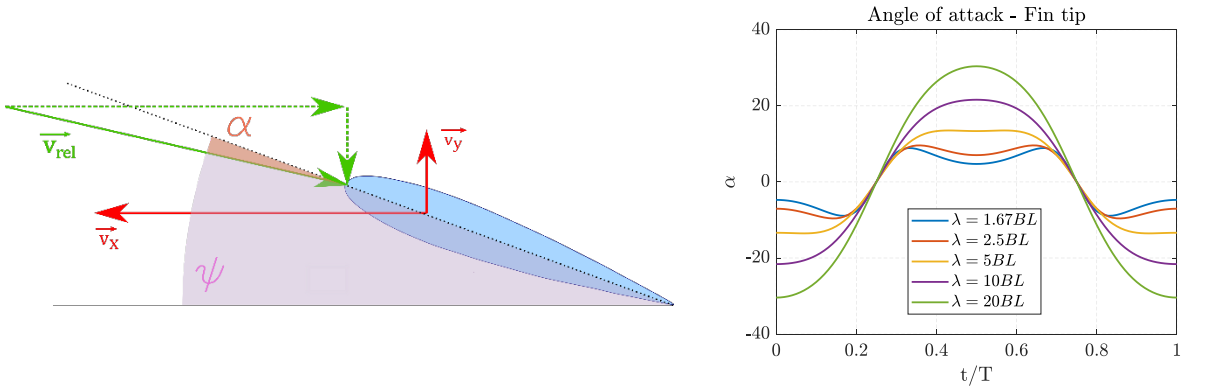

(a) – Angle of attack of a fin section

(b) - Variation of the angle of attack of a fin section at 90% of the fin span

Figure 20: Angle of attack

The angle of attack is also a key parameter governing the dynamics of the leading-edge vortex; an LEV is formed only when the fish swims with a long wavelength, i.e., with a high angle of attack, in accordance with Eldredge [30], which states that a high angle of attack is fundamental for the formation of the LEV.

6.4 Strouhal number

The Strouhal number for a swimming fish is defined as follows:

$$St = \frac{f\,A}{U} \tag{10}$$

where f is the flapping frequency, A is the peak-to-peak amplitude of the trailing edge of the fin, and U is the swimming velocity [23]. For a batoid fish, the trailing edge amplitude is variable along the span of the fin; thus, it is better to measure the vertical distance between two vortex cores directly from the wake. It results that this distance is the peak-to-peak amplitude of the farthest span of the fin before the beginning of the fin tip vortex. The Strouhal number for different wavelengths and frequencies is presented in Fig. 25. Since the steady-state velocity is proportional to frequency, the Strouhal number does not depend on frequency, whereas it varies with wavelength. The Strouhal number of the cownose ray swimming is between 0.2 and 0.4 for most of the simulated swimming modes. This result fits with observations by Fish [4], Eloy [23], and Taylor [31], and it is a remarkable confirmation of the ability of the model to catch and reproduce the real behavior of the cownose ray. Furthermore, for the simulation with $f = 1\text{Hz}$ and $\lambda = 2.5\,\text{BL}$, the most typical swimming parameters for the cownose ray, the Strouhal number is perfectly in the middle of this optimal range. For a greater wavelength, the Strouhal number decreases below 0.2, and the propulsive efficiency decreases. Conversely, the Strouhal number results to be higher and outside the optimal range for a short wavelength, although the energy efficiency is the highest among all the simulations. The efficiency trend with respect to wavelength suggests that the efficiency can increase indefinitely, reducing the wavelength. However, this is not possible in practice because it would induce a great deformation on the fin surface that could be impossible to achieve for a real fish.

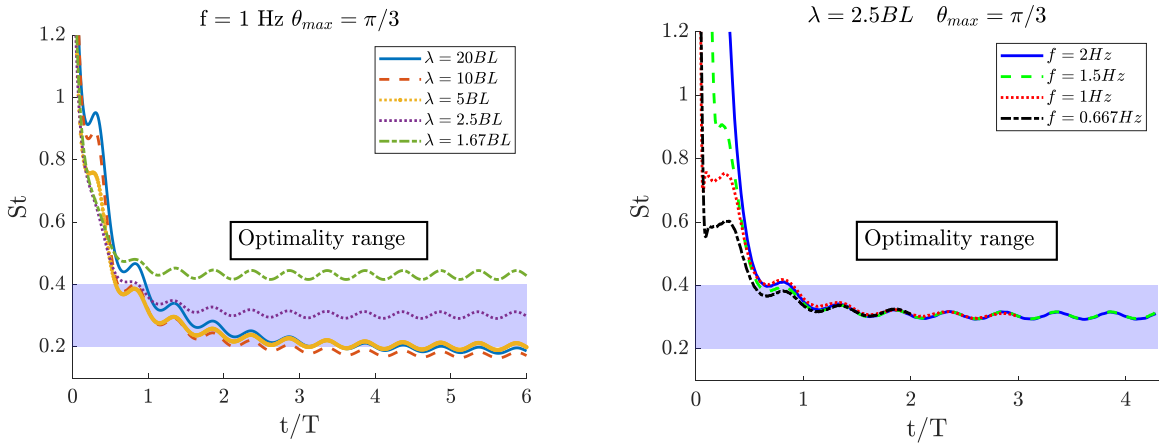

(a) – Strouhal number for different wavelengths **(b) – Strouhal number for different frequencies**

Figure 21: Strouhal number

7 CONCLUSION

A CFD model coupled with a dynamic solver has been developed, using a deformable overset grid. This method has been applied to simulate the swimming of a cownose ray with an imposed deformation on the fin, taken from the observations of the real fish made by biologists, and it could be applied for each fish once its motion is known.

The wake structure has been analyzed, highlighting the presence of vortices forming a reverse Karman street. This is related to thrust generation with an oscillatory motion, and it is present in the wake of the majority of fish. Furthermore, other vortices around the fin tips and near the center of the body have been put in evidence, and they have been related to the fins' motion. Such simulations have been carried out with different wavelengths and frequencies of fin motion, and the swimming performances have been compared. The presence of a leading-edge vortex has been highlighted for fin motion with a long wavelength; nevertheless, such a long wavelength is not typical of the movement of a cownose ray, and its energy efficiency is small. Despite the presence of a leading-edge vortex, the main contribution to thrust is given by the traveling wave pushing water in the opposite direction.

The steady-state velocity is proportional to frequency, and it is maximum for a particular wavelength value. The energy efficiency for a self-propelled body has been defined in a novel way; it has been found that it is remarkably high for the cownose ray and does not depend on frequency but only on wavelength. The calculated Strouhal number resulted in being in the same optimal range as other swimming and flying animals.

The developed model is a useful tool that will also be used to analyze the dynamics of maneuvering of batoid fishes and understand the effect of spanwise wave propagation on the fin. The results obtained could be a starting point for designing a bio-inspired underwater robot and for the choice of its kinematics and its motion law, as they reveal the effect of different swimming strategies on motion performances. A biomimetic AUV has been built and the fins have been designed with the aim of replicating this kind of motion, which this numerical analysis has revealed to be very efficient. The robot will be soon tested in water to assess the validity of this model.

The capabilities of the CFD model go beyond the study of the mechanism of forward swimming, as it can be deepened, including the influence of the amplitude of fin movement in this study. This model could also be improved, removing the constraints on vertical and lateral displacements and on rotations to explore the hydrodynamics of turning and diving maneuvers which are of great interest since batoid fishes display far better agility than traditional AUVs. In the long term, a study of the kinematics of fin movement of different fishes could be carried out, so to simulate their behavior, and to perform a comparative study of fish swimming performances, which could be useful to understand which are the most useful features that a bioinspired AUV should mimic.

REFERENCES

[1] J. Dabiri e M. Gordon, Animal Locomotion. Physical Principles and Adaptations, Boca Raton, FL, USA: Taylor & Francis Group, 2017.

[2] K. Moored, F. Fish, T. Kemp e H. Bart-Smith, «Batoid Fishes: Inspiration for the Next Generation of Underwater Robots,» *Mar. Technol. Soc. J.,* vol. 45, n. 4, pp. 99-109, 2011.

[3] R. Salazar, V. Fuentes e A. Abdelkefi, «Classification of Biological and Bioinspired Aquatic Systems: A Review,» *Ocean Eng.,* vol. 148, pp. 75-114, 2018.

[4] F. Fish, C. Schreiber, K. Moored, G. Liu, H. Dong e H. Bart-Smith, «Hydrodynamic Performance of Aquatic Flapping: Efficiency of Underwater Flight in the Manta,» *Aerospace,* vol. 3, n. 3, p. 20, 2016.

[5] G. Liu, Y. Ren, J. Zhu, H. Bart-Smith e H. Dong, «Thrust Producing Mechanisms in Ray-Inspired Underwater Vehicle Propulsion,» *Theor. Appl. Mech. Lett.,* vol. 5, n. 1, pp. 54-57, 2015.

[6] J. Zhan, Y. Gong e T. Li, «Effect of Angles of Attack on the Hydrodynamic Forces of Manta Ray,» in *Proceedings of the Eleventh Pacific/Asia Offshore*, Shanghai, 2014.

[7] N. Sharp, V. Hagen-Gates, E. Hemingway, M. Syme, J. Via, J. Feaster, J. Bayandor, S. Jung, F. Battaglia e A. Kurdila, «Computational Analysis of Undulatory Batoid Motion for Underwater Robotic Propulsion,» *ASME,* vol. FEDSM2014., 2014.

[8] X. Liu, T. Iwasaki e F. Fish, «Dynamic Modeling and Gait Analysis,» in *American Control Conference*, Washignton DC, USA, 2013.

[9] C. Wei-Shan, W. Zhi-Jun, L. Jun-Kao, S. Sheng-Jun e Z. Yang, «Numerical Simulation of Batoid Locomotion,» *J. Hydrodyn,* vol. 23, pp. 594-600, 2011.

[10] R. G. Bottom, I. Borazjani, E. L. Blevins e G. V. Lauder, «Hydrodynamics of Swimming in Stingrays: Numerical Simulations and the Role of the Leading-Edge Vortex,» *J. Fluid Mech.,* vol. 788, pp. 407-443, 2016.

[11] N. Thekketil e A. A. A. Sharma, «Three-Dimensional Biological Hydrodynamics Study on Various Types of Batoid Fishlike Locomotion,» *Phys. Rev. Fluids,* vol. 5, pp. 1-26, 2020.

[12] H. Huang, C. Sheng, J. Wu, G. Wu, C. Zhou e H. Wang, «Hydrodynamic Analysis and Motion Simulation of Fin and Propeller Driven Manta Ray Robot,» *Appl. Ocean. Res.,* vol. 108, p. 102528, 2021.

[13] M. Sfakiotakis, D. M. Lane e J. B. C. Davies, «Review of Fish Swimming Modes for Aquatic Locomotion,» *IEEE J. Ocean. Eng.,* vol. 24, n. 2, pp. 237-252, 1999.

[14] Y. Cai, S. Bi, G. Li, H. Hildre e H. Zhang, «From Natural Complexity to Biomimetic Simplification. the Realization of Bionic Fish Inspired by the Cownose Ray,» *IEEE Rob. Autom. Mag.,* vol. 26, n. 3, pp. 27-38, 2019.

[15] Y. Cai, S. Bi e L. Zhang, «Design and Implication of a Bionic Pectoral Fin Imitating Cow-Nosed Ray,» in *IEEE/RSJ International Conference on Intelligent Robots and Systems*, Taipei, Taiwan, 2010.

[16] G. R. Poulakis, «Reproductive Biology of the Cownose Ray in the Charlotte Harbor Estuarine System, Florida,» *Mar. Coastal Fish. Dyn., Manage. Ecosyst. Sci.,* vol. 5, n. 1, pp. 153-173, 2013.

[17] R. Russo, S. Blemker, F. Fish e H. Bart-Smith, «Biomechanical Model of Batoid (Skates and Rays) Pectoral Fins Predicts the Influence of Skeletal Structure on Fin Kinematics: Implications for Bio-Inspired Design,» *Bioinspiration & Biomimetics,* vol. 10, n. 4, p. 046002, 2015.

[18] K. Moored, P. Dewey, M. Leftwich, H. Bart-Smith e A. Smits, «Bioinspired Propulsion Mechanisms Based on Manta Ray Locomotion,» *Mar. Technol. Soc. J.,* vol. 45, n. 4, pp. 110-118, 2011.

[19] G. Shi, Q. Xiao, Q. Zhu e W. Liao, «Structure Interaction Modeling on a 3d Ray-Strengthened Caudal Fin,» *Bioinspiration & Biomimetics,* vol. 14, n. 3, p. 036012, 2019.

[20] M. Gazzola, M. Argentina e L. Mahadevan, «Scaling Macroscopic Aquatic Locomotion,» *Nat. Phys.,* vol. 10, n. 10, pp. 758-761, 2014.

[21] R. Clark e A. Smits, «Thrust Production and Wake Structure of a Batoid-Inspired Oscillating Fin,» *J. Fluid Mech.,* vol. 562, pp. 415-429, 2006.

[22] P. A. Dewey, A. Carriou e A. Smits, «On the Relationship Between Efficiency and Wake Structure of a Batoid-Inspired Oscillating Fin,» *J. Fluid. Mech,,* vol. 691, pp. 245-266, 2012.

[23] C. Eloy, «Optimal Strouhal Number for Swimming Animals,» *J. Fluids Struct.,* vol. 30, pp. 205-218, 2012.

[24] S. Siegel, J. Seidel, K. Cohen e T. McLaughlin, «A Cycloidal Propeller Using Dynamic Lift,» *AIAA,* p. 4232, 2007.

[25] I.Borazjani e M. Daghooghi, «The Fish Tail Motion Forms an Attached Leading Edge Vortex,» *Proc. R. Soc. B,* vol. 280, p. 20122071, 2013.

[26] H. Lu, K. S. Yeo e C. Chew, «Effect of Pectoral Fin Kinematics on Manta Ray Propulsion,» *Mod. Phys. Lett. B,* vol. 32, p. 1840025, 2018.

[27] A. Maertens, M. Triantafyllou e D. Yue, «Efficiency of Fish Propulsion,» *Bioinspiration & Biomimetics,* vol. 10, n. 4, p. 046013, 2015.

[28] R. Bale, M. Hao, A. Bhalla e N. Patankar, «Energy Efficiency and Allometry of Movement of Swimming and Flying Animals,» *Proc. Natl. Acad. Sci.,* vol. 111, n. 21, pp. 7517-7521, 2014.

[29] L. Rosemberger, «Pectoral Fin Locomotion in Batoid Fishes: Undulation Versus Oscillation,» *J. Exp. Biol.,* vol. 204, pp. 379-394, 2001.

30] J. D. Eldredge e A. R. Jones, «Leading-Edge Vortices: Mechanics and Modeling,» *Annu. Rev. Fluid Mech.,* vol. 51, n. 1, pp. 75-104, 2019.

[31] G. Taylor, «Simple Scaling Law Predicts Peak Efficiency in Oscillatory Propulsion,» *PNAS,* vol. 115, n. 32, pp. 8063-8065, 2018.

[32] J. M. Anderson, K. Streitlien, D. S. Barrett e M. S. Triantafyllou, «Oscillating Foils of High Propulsive Efficiency,» *J. Fluid Mech.,* vol. 360, pp. 41-72, 1998.

[33] T. Schnipper, A. Andersen e T. Bohr, «Vortex Wakes of a Flapping Foil,» *J. Fluid Mech.,* vol. 633, pp. 411-423, 2009.